Data report: Permeability measurements under confining pressure, Legs 315 and 316, Nankai Trough

Thierry REUSCHLE

Ecole et Observatoire des Sciences de la Terre, Institut de Physique du Globe de Strasbourg (CNRS/Université de Strasbourg UMR 7516), 5 rue René Descartes, 67084 Strasbourg Cedex, France

ABSTRACT

Permeability of six samples from sites C0001 and C0006 were measured in a triaxial cell under effective hydrostatic confining pressure from 1 to 30 MPa. Our results indicate that the initial permeability at 1 MPa of effective confining pressure ranges from 4.6×10^{-18} to 1.8×10^{-19} m^2 depending on depth. Actually permeability decreases with increasing depth also corresponding to a decrease of porosity from 62 to 43%. The permeability *vs.* depth trend is similar for both sites. When the effective confining pressure is increased from 1 to 30 MPa, the permeability decreases for all samples, a decrease interpreted by microfracture closure. However this trend shows some variability indicating a finer microstructural control depending on the lithological origin of the sample.

INTRODUCTION

When analysing deformation processes in accretionary complexes like the Nankai one, one has to take into account several time scales. One important time scale is given by the competition between two kinetics: the first one is related to the eventual pore pressure build-up linked to the pore fluid trapping during the tectonic loading of the subduction zone, the second one is related to the ability for the pore fluid to flow out of the system, thus avoiding any effective confining stress decrease that would enhance instability of the system. The latter is controlled by the permeability of the rock. Permeability measurements on samples from the Nankai accretionary complex have been already performed without pressure confinement (Taylor & Fisher 1993) or at low confining pressure (< 1 MPa) (Gamage & Screaton 2003; Karig 1993). Measurements of permeability under 1 - 5 MPa effective confining pressure give lower values (Byrne *et al.* 1993). More recently, Bourlange *et al.* (2004) reported permeability measurements performed in the 0.5 - 2.5 MPa range in a triaxial cell with the main purpose of approaching *in situ* stress conditions. Overall, their results indicate that permeability decreases from 10^{-18} to 10^{-19} m^2 with effective confining pressure up to 1.5 MPa. When the effective pressure is then increased from 1.5 to 2.5 MPa, permeability is roughly constant ($\sim 1 - 4 \times 10^{-19}$ m^2) indicating a threshold pressure beyond which fracture closure is stopped. However, measurements at low effective pressure were too dispersed to yield a precise general relationship between pressure, permeability and thus crack geometrical parameters.

In the present report, we present permeability measurements performed in the range 1 - 30 MPa in a hydrostatic cell with the main goal of refining this relationship, thus giving some new insights in the pressure dependence of microstructural characteristics of samples having various lithological origins.

EXPERIMENTAL PROCEDURE

Permeability measurements were performed on two sets of samples stemming of sites C0001 (Leg 315) and C0006 (Leg 316) at various depths (Fig. 1). For each depth level two cylindrical specimens (20 mm in diameter and 15 - 20 mm in length) were drilled out of the initial cores in a vertical direction (Fig. 2): one for the porosity determination, the second for the permeability measurement. The porosity of the unstressed samples was measured by using the triple-weighing method: the successive measurements of the initial saturated, saturated immersed and dry specimen masses lead to the determination of the connected porosity. Table 1 summarizes porosity data for the tested samples and on figure 3 we illustrate the depth-dependence of porosity. This dependency compares well with porosity data obtained on-board and derived from resistivity logs (Expedition 314 Scientists 2009; Expedition 316 Scientists 2009).

Permeability measurements were carried out, at room temperature, in a 200 MPa hydrostatic pressure cell equipped with a pore fluid pressure circuit (Fig. 4). The whole apparatus was thermally regulated to keep pressures constant in the absence of imposed pressure changes. The samples were isolated from the confining pressure fluid by a Viton jacket clamped on the end pieces connected to the pore fluid circuit. Pore fluid and confining pressures P_P and P_C were controlled separately. During the experiments, an effective pressure (P_C - P_P) of at least 1 MPa was maintained on the sample to ensure a uniform contact of the jacket onto the specimen, and to avoid any leaking. All the experiments were run on the initial saturated samples.

The initial pressure conditions for all samples were P_C = 3 MPa and P_P = 2 MPa in order to be able to compare their hydraulic conductivities. Once the pressures were constant, permeabilities were measured using a pulse decay method (Bernabé 1987; Brace 1984). After closing the isolating valve between the upstream and downstream pore pressure circuits, a small step change of differential pore fluid pressure $\Delta P_P = P_{up} - P_{down}$ was imposed in the upstream pore pressure section. Both pressures were then free to return to equilibrium through the sample. When the compressive

storage in the sample is much smaller than the compressive storage in the pore fluid circuits, the differential pore pressure decay ΔP_P is approximately exponential and the decay time inversely proportional to the permeability as shown by the following equations (Hsieh *et al.* 1981):

$$\Delta P_P(t) \propto \exp(-\alpha t) \qquad (1)$$

and

$$\alpha = \frac{Ak(C_u + C_d)}{\mu L C_u C_d} \qquad (2)$$

where t is the time, A and L are the section and length of the sample respectively, μ is the viscosity of the pore fluid (10^{-3} Pa.s at 20°C), k is the permeability, C_u and C_d are the compressive storages of the upstream and downstream pore pressure circuits, defined as the ratios of the change of fluid volume to the corresponding pore pressure variation ($C = \partial V/\partial P_P$). They are physical constants of the apparatus and have been experimentally determined: C_u = 3.957 10^{-9} m^3/MPa and C_d = 4.828 10^{-9} m^3/MPa. On figure 5 we show an example of pore pressure evolution with time (Fig. 5a) and the resulting differential pore pressure decay (Fig. 5b). As one can see, the exponential law is a rather good approximation leading to well constrained permeability values.

Measurements were performed with this method on all samples at increasing levels of effective confining pressure P_C - P_P from 3 to 30 MPa, with 2 MPa increase steps for the confining pressure P_C and a constant pore pressure P_P = 2 MPa. Since the pulse decay method requires small initial pore pressure difference (10 %) compared to the equilibrium pore pressure, we applied an initial 0.5 MPa positive pulse to the upstream pore circuit, but we restricted our analysis to the final 0.2 MPa portion of the ΔP_P decay curve.

RESULTS

Permeability measurements were performed on samples referenced in Table 1 using the procedure described above. One series of measures, including equilibration times between permeability measurements lasted about two months. On figure 6 we have plotted permeability data at the initial pressure conditions (P_C = 3 MPa and P_P = 2 MPa) as a function of depth for both sites. This diagram gives us a good insight into the permeability *vs.* depth trend: permeability decreases as depth is increased and the trend is similar for both sites. Moreover the permeability at site C0006 is lower than the permeability at site C0001 for equivalent depths. This point is easily explained by the lower porosity encountered at site C0006: figure 7 illustrates the good correlation between porosity and permeability for all samples. The permeability trend with depth observed on site C0001 is quite consistent with data obtained by Likos *et al.* (2010). Our measurements are however lower than their data, a difference that can be explained by the lower effective stress (0.55 MPa) applied to the samples by these authors.

Indeed our measurements indicate a permeability decrease over 1.5 order of magnitude when an increasing effective confining pressure up to 30 MPa is applied. Figure 8 summarizes the obtained data for site C0001 (Fig. 8a) and site C0006 (Fig. 8b). As one can see the decrease of permeability is apparent for all samples but the shape of the curve differs from one sample to the other reflecting variability in their microstructural content. The decrease of permeability with the increase in effective stress is interpreted as fracture closure. As suggested by Walsh (1981) a linear relationship may be found between permeability and effective pressure. This is rather the case for sample 316C6F19R03 and 316C6E31X04 (Fig. 8b) but does not hold for the other samples. A possible explanation may be the fact that the effective pressure definition we have used in our study does not hold for clay-rich rocks (Al-Wardy & Zimmerman 2003) or a better description of fracture roughness (Gavrilenko & Guéguen 1989) should be introduced to take into account the fact that rough fractures do not close even at higher effective pressures.

CONCLUSIONS

Permeability measurements were performed on samples from sites C0001 and C0006 in a triaxial cell under effective hydrostatic confining pressure ranging from 1 to 30 MPa. The pulse decay method was employed and showed an exponential trend of the differential pore pressure with time, leading to well constrained permeability data. A decrease of the initial permeability at 1 MPa effective pressure from 4.6×10^{-18} to 1.8×10^{-19} m^2 with increasing depth was observed on both sites and is well correlated with the porosity trend. When the effective confining pressure is increased from 1 to 30 MPa, the permeability decreases for all samples, which is interpreted by microfracture closure. However this trend shows some variability indicating a finer microstructural control depending on the lithological origin of the sample.

ACKNOWLEDGEMENTS

We would like to thank P. Henry (site C0001) and L. Louis (site C0006) for sample supply. We also thank J.-D. Bernard for technical advice during the test period.

REFERENCES

Al-Wardy, W. & Zimmerman, R.W., 2003. Effective stress law for the permeability of clay-rich sandstones, in *16th ASCE Engineering Mechanics Conference*, pp. 1-5, University of Washington, Seattle.

Bernabé, Y., 1987. A wide range permeameter for use in rock physics. *Int J Rock Mech Min Sci Geomech Abstr*, **24**, 309-315.

Bourlange, S., Jouniaux, L. & Henry, P., 2004. Data report: Permeability, compressibility, and friction coefficient measurements under confining pressure and strain, Leg 190, Nankai trough,

in *Proc. ODP, Sci. Results*, 190/196, pp. 1-16, ed. Mikada, H., Moore, G.F., Taira, A., Becker, K., Moore, J.C. & Klaus, A.

Brace, W.F., 1984. Permeability of crystalline rocks: new in situ measurements. *J Geophys Res*, **89**, 4327-4330.

Byrne, T., Maltman, A., Stephenson, E., Soh, W. & Knipe, R., 1993. Deformation structures and fluid flow in the toe region of the Nankai accretionary prism, in *Proc. ODP, Sci. Results*, 131, pp. 83-101, ed. Hill, I.A., Taira, A., Firth, J.V. & *et al.*, College Station, TX (Ocean Drilling Program).

Expedition 314 Scientists, 2009. Expedition 314 Site C0001, in *Proc. IODP*, 314/315/316, ed. Kinoshita, M., Tobin, H., Ashi, J., Kimura, G., Lallement, S., Screaton, E.J., Curewitz, D., Masago, H., Moe, K.T. & the Expedition 314/315/316 Scientists, Washington, DC (Integrated Ocean Drilling Program Management International, Inc.), doi:10.2204/iodp.proc.314315316.113.2009.

Expedition 316 Scientists, 2009. Expedition 316 Site C0006, in *Proc. IODP*, 314/315/316, ed. Kinoshita, M., Tobin, H., Ashi, J., Kimura, G., Lallement, S., Screaton, E.J., Curewitz, D., Masago, H., Moe, K.T. & the Expedition 314/315/316 Scientists, Washington, DC (Integrated Ocean Drilling Program Management International, Inc.), doi:10.2204/iodp.proc.314315316.134.2009.

Gamage, K. & Screaton, E., 2003. Data Report: Permeabilities of Nankai accretionary prism sediments, in *Proc. ODP, Sci. Results*, 190/196, pp. 1-22, ed. Mikada, H., Moore, G.F., Taira, A., Becker, K., Moore, J.C. & Klaus, A.

Gavrilenko, P. & Guéguen, Y., 1989. Pressure dependence of permeability: a model for cracked rocks. *Geophys. J. Int.*, **98**, 159-172.

Hsieh, P.A., Tracy, J.V., Neuzil, C.E., Bredehoeft, J.D. & Silliman, S.E., 1981. A transient laboratory method for determining the hydraulic properties of 'tight' rocks- I. Theory. *Int J Rock Mech Min Sci Geomech Abstr*, **18**, 245-252.

Karig, D.E., 1993. Reconsolidation tests and sonic velocity measurements of clay-rich sediments from the Nankai Trough, in *Proc. ODP, Sci. Results*, 131, pp. 247-260, ed. Hill, I.A., Taira, A., Firth, J.V. & et al., College Station, TX (Ocean Drilling Program).

Likos, W.J., Yue, L, Guo, J Underwood, M, 2010. Laboratory permeability characteristics: site C0001. *Geochemistry Geophysics Geosystems*, submitted.

Taylor, E. & Fisher, A., 1993. Sediment permeability at the Nankai accretionary prism, Site 808, in *Proc ODP, Sci. Results*, 131, pp. 235-245, ed. Hill, I.A., Taira, A., Firth, J.V. & et al., College Station, TX (Ocean Drilling Program).

Walsh, J.B., 1981. Effect of pore pressure and confining pressure on fracture permeability. *Int. J. Rock Mech. Min. Sci. Geomech. Abstr.*, **18**, 429-435.

Leg 315	315C1F18H06	315C1H8R01	315C1H25R01
Depth (m bsf)	225	297	448
Porosity (%)	61.7	58.2	50.6
Leg 316	316C6E28X01	316C6E31X04	316C6F19R03
Depth (m bsf)	201	232	564
Porosity (%)	48.2	43	42.9

Table 1. Porosity data for the tested samples as a function of depth.

Figure captions

Figure 1. Lithostratigraphy and location of samples at sites C0001 and C0006.

Figure 2. Sample 315C1F18H06 before permeability measurements.

Figure 3. Porosity *vs.* depth diagram for the tested samples.

Figure 4. Experimental set-up. The specimen Sp is inserted in a jacket clamped on end-pieces. Confining pressure P_C, upstream and downstream pore fluid pressure P_{up} and P_{down} circuits are in solid lines.

Figure 5. Example of pore fluid pressure evolution during a permeability test using the pulse decay method. Test was run on sample 315C1F18H06 at 30 MPa effective pressure. **(a)** The two curves correspond to the evolution of pore pressure at both ends of the sample. **(b)** The differential pore pressure follows an exponential decay law leading to a permeability of 6.22 10^{-20} m^2.

Figure 6. Permeability data at initial pressure conditions (P_C = 3 MPa and P_P = 2 MPa) as a function of depth for both sites.

Figure 7. Permeability *vs.* porosity data for all tested samples.

Figure 8. Permeability data as a function of effective confining pressure for samples of **(a)** site C0001 and **(b)** site C0006.

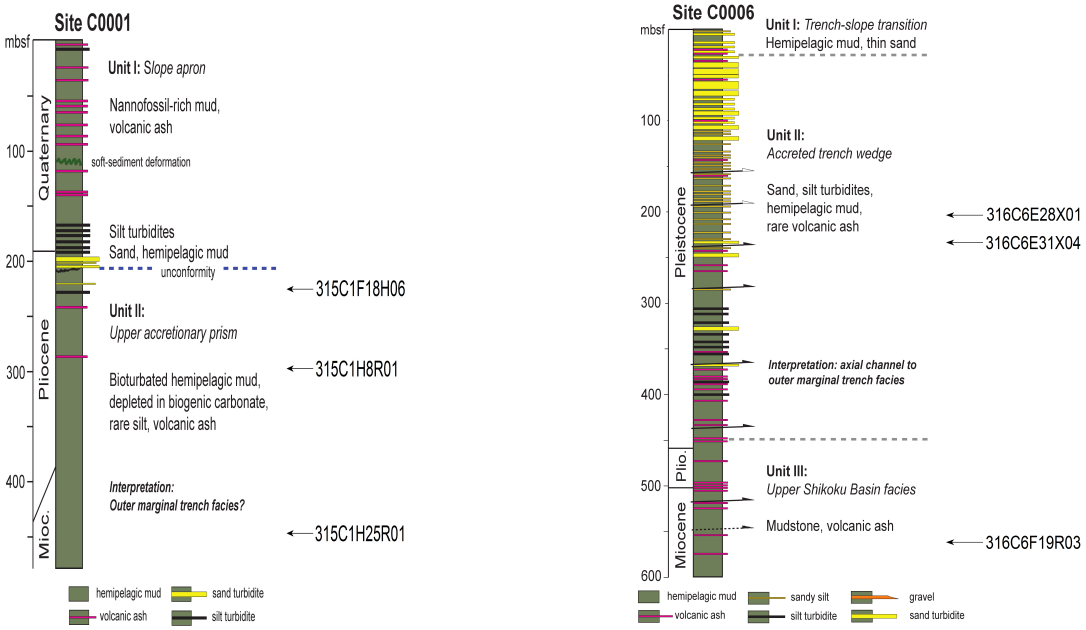

Figure 1

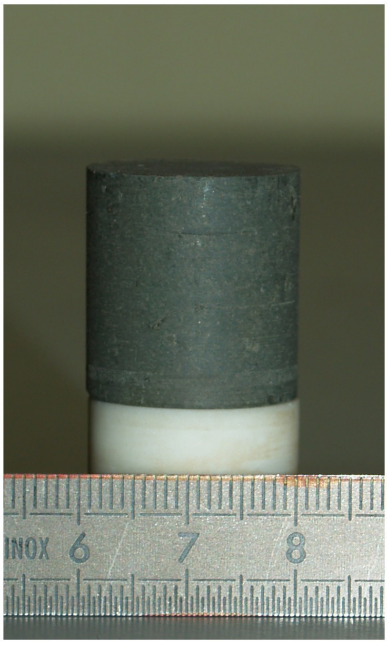

Figure 2

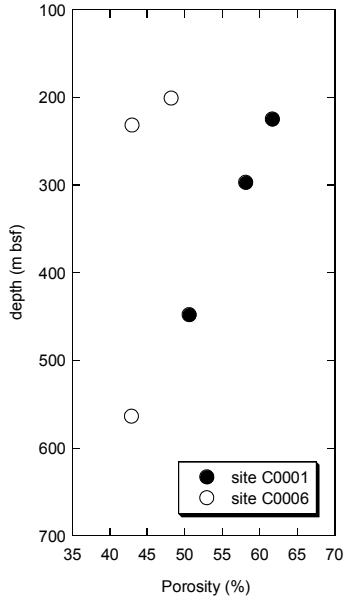

Figure 3

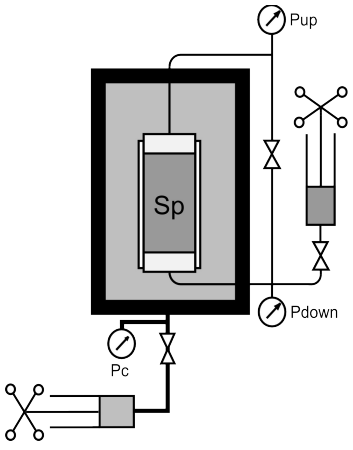

Figure 4

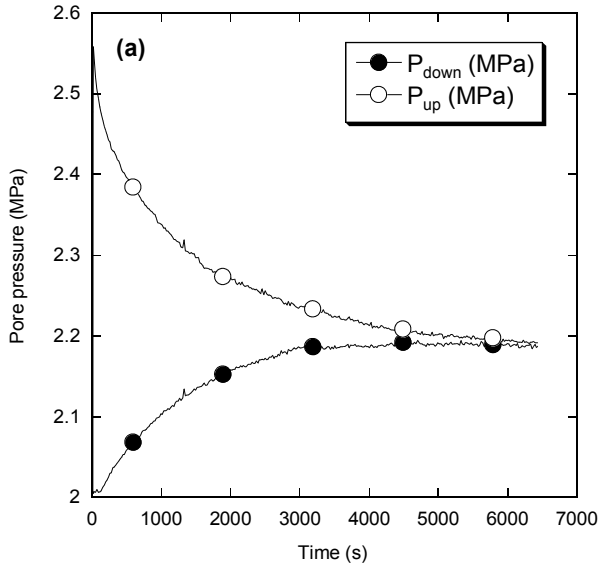
(a)
P_{down} (MPa)
P_{up} (MPa)
Pore pressure (MPa)
Time (s)
2.6
2.5
2.4
2.3
2.2
2.1
2
0
1000
2000
3000
4000
5000
6000
7000

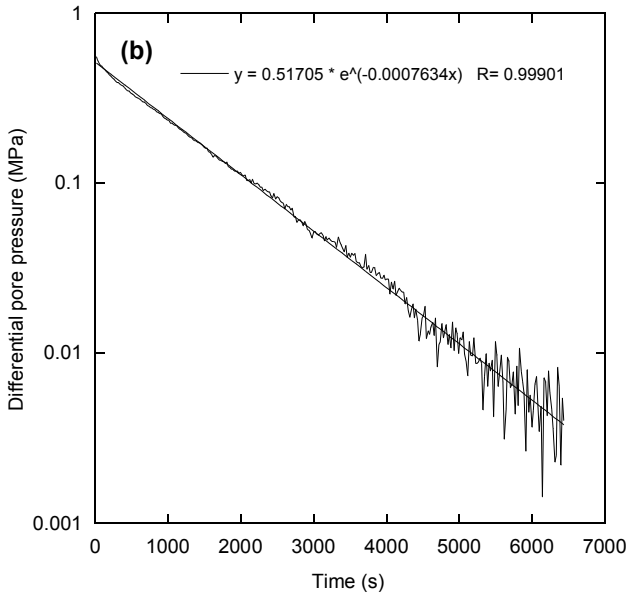
(b)
y = 0.51705 * e^(-0.0007634x) R= 0.99901
Differential pore pressure (MPa)
Time (s)
1
0.1
0.01
0.001
0
1000
2000
3000
4000
5000
6000
7000

Figure 5

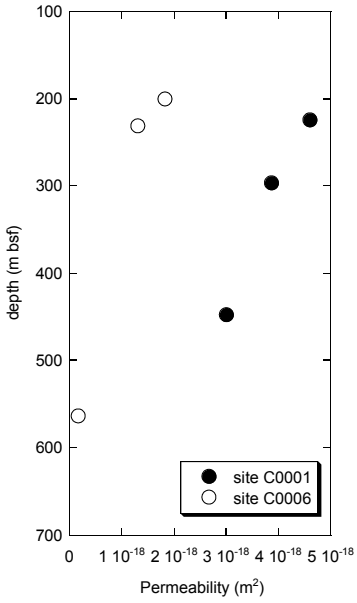

Figure 6

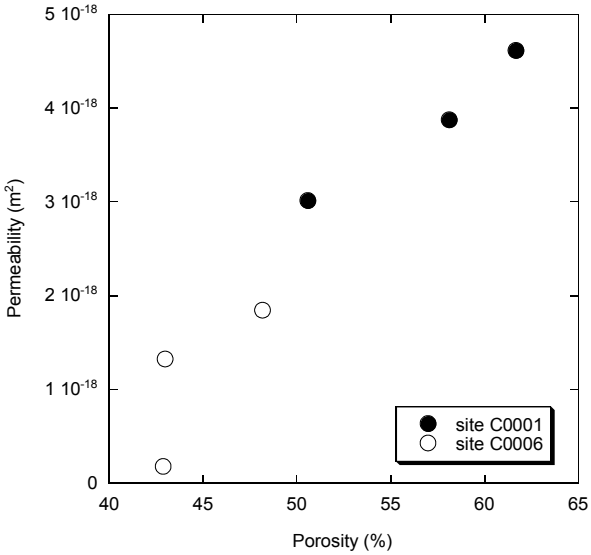

Figure 7

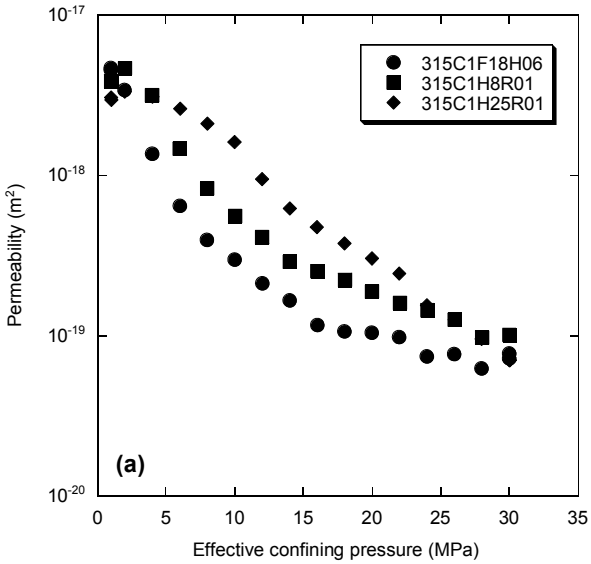
315C1F18H06
315C1H8R01
315C1H25R01
(a)
Permeability (m²)
Effective confining pressure (MPa)

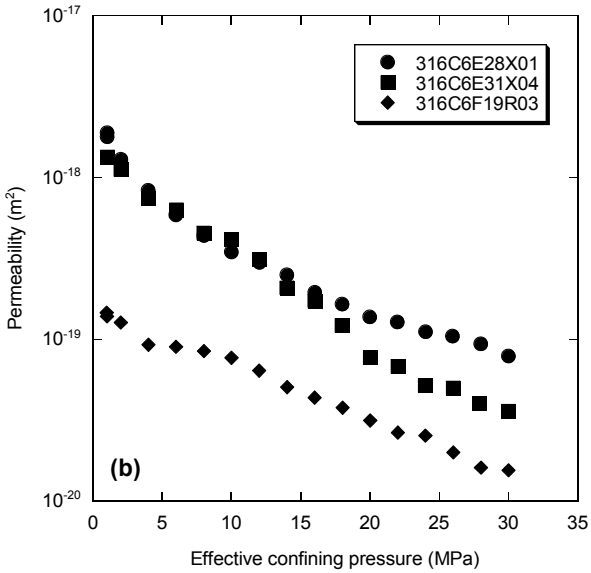
316C6E28X01
316C6E31X04
316C6F19R03
(b)
Permeability (m²)
Effective confining pressure (MPa)

Figure 8